Gold-Tin Ordering in $SrAu_2Sn_2$

Christian Schwickert, Birgit Gerke and Rainer Pöttgen

Institut für Anorganische und Analytische Chemie, Universität Münster, Corrensstrasse 30, 48149 Münster, Germany

Reprint requests to R. Pöttgen. E-mail: pottgen@uni-muenster.de

Z. Naturforsch. **2014**, *69b*, 767 – 774 / DOI: 10.5560/ZNB.2014-4097
Received May 6, 2014

Samples of the solid solutions $SrAu_xSn_{4-x}$ ($1.7 \leq x \leq 2.2$) were obtained by high-frequency melting of the elements in sealed niobium ampoules. Powder and single-crystal X-ray data confirmed the $CaBe_2Ge_2$-type structure, space group $P4/nmm$. The structures of $SrAu_{1.76}Sn_{2.24}$, $SrAu_2Sn_2$, $SrAu_{2.16}Sn_{1.84}$ (crystal A), $SrAu_{2.16}Sn_{1.84}$ (crystal B), and $SrAu_{2.22}Sn_{1.78}$ were refined from single-crystal diffractometer data. Only the $SrAu_2Sn_2$ crystal shows complete Au-Sn ordering while all other crystals show substantial mixed occupancies on the four crystallographically independent sites of the polyanionic networks in which the strontium atoms fill cages of coordination number 16. Temperature-dependent susceptibility measurements have revealed diamagnetism for $SrAu_2Sn_2$. ^{119}Sn Mössbauer spectroscopic data of a bulk $SrAu_2Sn_2$ sample have resolved the tetrahedral and square-pyramidal tin sites but point to substantial Au-Sn disorder.

Key words: Stannide, $CaBe_2Ge_2$ Structure, Gold, Intermetallics, Mössbauer Spectroscopy

Introduction

Most metals react with a tin flux forming a manifold of binary and ternary stannides [1]. Tin shows an excellent wettability for many transition metals, and especially the stannides of the electron-rich transition metals are important materials in microelectronics as solder/metal interfaces [2]. The most relevant stannides are Cu_6Sn_5, Cu_3Sn, and Ni_3Sn_4, but presently the gold stannides Au_5Sn, AuSn and $AuSn_4$ have become very important in high-quality devices with corrosion-resistant gold supply cables.

Although the binary gold stannides find application in such devices, only few data are known for ternary stannides, especially with the alkaline earth metals. So far only the stannides MgAuSn [3], CaAuSn [4], $Ca_{14}Au_{46}Sn_5$ [5], the icosahedral quasicrystal approximants $Ca_3Au_{14.36}Sn_{4.38}$ and $Ca_{13}Au_{47.2}Sn_{28.1}$ [6], SrAuSn [7], $SrAuSn_2$ [8], the solid solutions $SrAu_xSn_{4-x}$ ($1.3 \leq x \leq 2.2$) [9], and BaAuSn [7] have been reported. Gold-tin ordering in such stannides is driven by the formation of strong covalent Au–Sn bonds with lengths close to the sum of the covalent radii for gold and tin of 274 pm [10]. Examples are CaAuSn (273 – 278 pm) [4] or SrAuSn (279 – 286 pm) [7]. Within the small range of the solid solutions $SrAu_xSn_{4-x}$ ($1.3 \leq x \leq 2.2$), such a gold-tin ordering is possible for the composition $SrAu_2Sn_2$. The powder diffraction data of Tkachuk and Mar pointed to $BaAl_4$-related subcell structures for all investigated samples [9], and no hints for complete ordering were obtained on the basis of powder diffraction. However, electronic structure calculations have pointed to higher stability by 0.27 eV per formula unit for a fully ordered $CaBe_2Ge_2$-type phase as compared to the $ThCr_2Si_2$ ordering variant.

Several of the $BaAl_4$-related phases show extended solid solutions, and thus one can effectively vary the magnetic properties of a given material. Nevertheless, whenever possible, nature tends to ordering of the atoms and/or vacancies in such structures. Some complex ordering patterns have recently been studied on the basis of group-subgroup schemes for $Ce_3Pd_6Sb_5$ ($\equiv CePd_2Sb_{1.667}\square_{0.333}$) and $Yb_5Cu_{11}Sn_8$ ($\equiv YbCu_{2.20}Sn_{1.60}\square_{0.20}$) [10], $Ce_8Rh_{17}Sb_{14}$ ($\equiv CeRh_{2.13}Sb_{1.75}\square_{0.12}$) [11], $SrPdGa_3$ [12], and the modulated stannide $SrPt_{1.833}\square_{0.167}Sn_2$ [13].

Reinvestigation of the gold-tin ordering in the solid solutions $SrAu_xSn_{4-x}$ indeed revealed the $CaBe_2Ge_2$ type for $SrAu_2Sn_2$. The structure refinement, magnetic

properties, and the results of a ^{119}Sn Mössbauer spectroscopic study of this stannide are reported herein.

Experimental

Synthesis

The targeted synthesis of samples of the solid solutions $SrAu_xSn_{4-x}$ ($1.7 \leq x \leq 2.2$) was performed using strontium rods (Johnson Matthey, > 99.9 %), gold shots (Allgussa AG, 99.9 %) and tin granules (Merck, > 99.99 %). Suitable strontium pieces were mechanically cleaned from surface impurities under dried paraffin oil and cleaned with cyclohexane before being stored in Schlenk tubes under a purified (titanium sponge 900 K, silica gel, molecular sieves) argon atmosphere.

The educts were weighted in niobium ampules in the ideal stoichiometric ratios and arc welded [14] under reduced argon pressure (*ca.* 700 mbar). Polycrystalline samples were obtained by placing the ampoules in a water-cooled sample chamber of an induction furnace [15] (Typ TIG 2.5/300, Hüttinger Elektronik, Freiburg, Germany) and rapidly heating to approx. 1350 K. After 30 min the temperature was slowly (20 K min^{-1}) reduced to 950 K followed by two hours of annealing. The reaction mixtures were quenched by shutting off the high-frequency generator. Single crystals were obtained from reactions in a resistance furnace by slowly (12 h) heating the samples to 1150 K followed by annealing for 12 h. The samples were then slowly cooled (96 h) to 650 K and in order to improve crystal quality annealed for 120 h before being cooled to ambient temperature by radiative heat loss. In order to protect the niobium ampoules from oxidation, they were sealed in evacuated silica tubes prior to the reaction.

The resulting samples are brittle and exhibit silvery luster while ground powders appear light grey. No reaction with the container material was evident, and the resulting samples are stable in air over months.

EDX data

Semiquantitative EDX analyses of single crystals of $SrAu_xSn_{4-x}$ studied on the diffractometer were carried out in variable pressure mode with a Zeiss EVO® MA10 scanning electron microscope with SrF_2, Au and Sn as standards. The experimentally observed average compositions (*cf.* Table 2) were close to the ideal ones, and the high standard deviations account for the variations in the point analyses on various parts of the irregularly shaped (shell-like fracture) crystals. No impurity elements heavier than sodium (detection limit of the instrument) were detected.

X-Ray diffraction

The powdered $SrAu_xSn_{4-x}$ samples were studied by X-ray diffraction (Guinier technique: Fujifilm BAS-1800 imaging plate detector, CuK_{α_1} radiation) with α-quartz (a = 491.30, c = 540.46 pm) as an internal standard. The lattice parameters (Table 1) were obtained from least-squares refinements and intensity calculations [16] ensuring correct indexing. The single-crystal and powder lattice parameters agreed well and are comparable with those of the $BaAl_4$-type representatives published in the literature [9] (Fig. 1 and Table 1).

Irregularly shaped single-crystal fragments of $SrAu_{1.76}Sn_{2.24}$, $SrAu_2Sn_2$, $SrAu_{2.16}Sn_{1.84}$ (crystal A and crystal B)

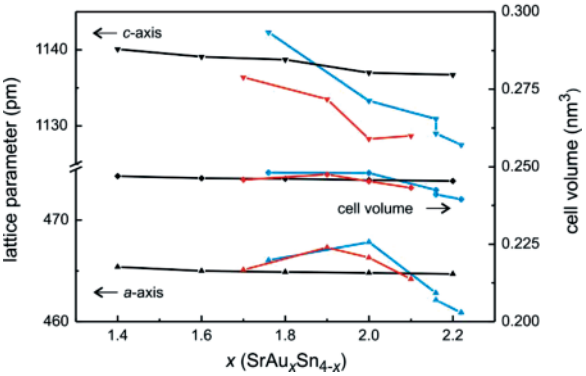

Fig. 1 (color online). Lattice parameters and cell volumes within the solid solutions $SrAu_xSn_{4-x}$ with $CaBe_2Ge_2$-type structure. Single-crystal data (blue), Guinier-powder data (red) and $ThCr_2Si_2$-type representatives published in literature [9] (black).

Table 1. Lattice parameters (Guinier technique) of the stannides $SrAu_xSn_{4-x}$, space group $P4/nmm$, compared with the $ThCr_2Si_2$-type representatives published in the literature.

Compound	a (pm)	c (pm)	V (nm^3)	Reference
$SrAu_{1.4}Sn_{2.6}$	465.4(1)	1140.1(4)	0.2470	[9]
$SrAu_{1.6}Sn_{2.4}$	465.03(9)	1139.1(4)	0.2463	[9]
$SrAu_{1.7}Sn_{2.3}$	465.10(8)	1136.4(3)	0.2458	this work
$SrAu_{1.76}Sn_{2.24}$[a]	466.04(3)	1142.3(1)	0.2481	this work
$SrAu_{1.8}Sn_{2.2}$	464.9(1)	1138.7(4)	0.2461	[9]
$SrAu_{1.9}Sn_{2.1}$	467.4(2)	1133.5(5)	0.2476	this work
$SrAu_2Sn_2$	464.8(2)	1137.0(8)	0.2457	[9]
$SrAu_2Sn_2$	466.30(6)	1128.3(2)	0.2453	this work
$SrAu_2Sn_2$[a]	467.84(9)	1133.3(2)	0.2480	this work
$SrAu_{2.1}Sn_{1.9}$	464.16(6)	1128.6(2)	0.2432	this work
$SrAu_{2.16}Sn_{1.84}$[a]	462.83(3)	1130.9(1)	0.2423	this work
$SrAu_{2.16}Sn_{1.84}$[a]	462.12(8)	1129.0(1)	0.2411	this work
$SrAu_{2.2}Sn_{1.8}$	464.7(1)	1136.7(6)	0.2454	[9]
$SrAu_{2.22}Sn_{1.78}$[a]	460.90(9)	1127.5(2)	0.2395	this work

[a] Single-crystal data.

Table 2. Single-crystal data and structure refinement for different $SrAu_xSn_{4-x}$ crystals, $CaBe_2Ge_2$ type, space group $P4/nmm$, $Z = 2$.

Refined composition	$SrAu_{1.76}Sn_{2.24}$	$SrAu_2Sn_2Sr$	$Au_{2.16}Sn_{1.84}$ crystal A	$SrAu_{2.16}Sn_{1.84}$ crystal B	$SrAu_{2.22}Sn_{1.78}$
EDX composition (±8 at.-%)	17 : 39 : 44	17 : 44 : 39	17 : 47 : 36	12 : 50 : 38	17 : 49 : 34
Formula weight, g mol^{-1}	700.3	719.0	731.7	731.1	736.3
Unit cell dimensions					
a, pm	466.04(3)	467.84(9)	462.83(3)	462.12(8)	460.90(9)
c, pm	1142.3(1)	1133.3(2)	1130.9(1)	1129.0(1)	1127.5(2)
Cell volume V, nm^3	0.2481	0.2480	0.2423	0.2411	0.2395
Calculated density, g cm^{-3}	9.37	9.62	10.03	10.07	10.21
Crystal size, μm^3	$60 \times 80 \times 80$	$30 \times 30 \times 60$	$30 \times 50 \times 100$	$20 \times 40 \times 80$	$20 \times 50 \times 50$
Transmission ratio (min/max)	0.066/0.212	0.043/0.165	0.332/0.738	0.022/0.233	0.015/0.096
Diffractometer	IPDS-II	IPDS-II	IPDS-II	IPDS-II	STADIVARI
Detector distance, mm	60	60	60	60	40
Exposure time, min per frame	6	8	7	7	0.03
ω-range/increment, deg	0–180/1.0	0–180/1.0	0–180/1.0	0–180/1.0	–
Integr. param. A/B/EMS	13.6/3.4/0.014	13.3/3.0/0.012	12.9/3.2/0.012	13.0/2.8/0.015	7.7/ − 5.0/0.018
Absorption coefficient, mm^{-1}	73.5	79.4	85.3	85.5	87.8
$F(000)$, e	578	592	602	603	606
θ range for data collection, deg	3–35	3–36	3–35	3–35	3–32
Range in hkl	±7, ±7, ±18	±7, ±7, ±18	±7, ±7, ±18	±7, ±7, ±18	±6, ±6, ±16
Total no. of reflections	7464	8166	15771	9577	7911
Independent reflections/R_{int}	374/0.0958	391/0.1548	364/0.1330	363/0.0577	292/0.0759
Reflections with $I > 3\,\sigma(I)/R_\sigma$	309/0.0154	109/0.0916	324/0.0089	264/0.0127	231/0.0073
Data/ref. parameters	374/16	391/15	364/17	363/18	292/17
Goodness-of-fit on F^2	1.89	0.92	1.97	1.49	2.11
R/wR for $I > 3\,\sigma(I)$	0.0361/0.0704	0.0245/0.0416	0.0351/0.0645	0.0237/0.0529	0.0273/0.0633
R/wR for all data	0.0490/0.0725	0.0930/0.0459	0.0451/0.0668	0.0435/0.0570	0.0324/0.0700
Extinction coefficient	2669(169)	60(20)	4100(400)	1130(90)	108(13)
Largest diff. peak/hole, e Å^{-3}	5.40/−5.62	0.45/−0.45	6.25/−7.28	3.33/−4.79	1.87/−2.66
Absorption correction	numerical	numerical	numerical	numerical	spheric

and $SrAu_{2.22}Sn_{1.78}$ were selected from the bulk samples by mechanical separation and glued to thin quartz fibers using beeswax. Their quality was checked on a Buerger camera (using white Mo radiation). The intensity data collections were performed on a Stoe IPDS-II image plate system (graphite-monochromatized Mo radiation; $\lambda = 71.073$ pm) in oscillation mode and on a Stoe StadiVari (μ-source, MoK_α radiation, $\lambda = 71.073$ pm; oscillation mode) diffractometer. All data sets were subjected to a numerical absorption correction, and in the case of the StadiVari scaling of the data set in combination with a spherical absorption correction was applied. The relevant crystallographic parameters as well as details on the data collections and evaluations are listed in Table 2.

Structure refinements

The four data sets showed primitive tetragonal Bravais lattices, and their systematic extinctions agreed with space group $P4/nmm$. This is in contrast to the published data for the solid solution [9], where only body-centered cells ($BaAl_4$ type [17]) were observed. Our hkl layers (Fig. 2, a $hk3$ layer of $SrAu_{1.76}Sn_{2.24}$ as an example) as well as the powder diffraction patterns (Fig. 3, experimental diffraction pattern of $SrAu_2Sn_2$) clearly showed superstructure reflections confirming space group $P4/nmm$, a *klassengleiche* subgroup of $I4/mmm$.

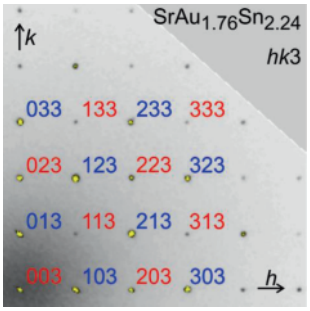

Fig. 2 (color online). $hk3$ layer of the $SrAu_{1.76}Sn_{2.24}$ data set. Superstructure reflections are drawn in red color.

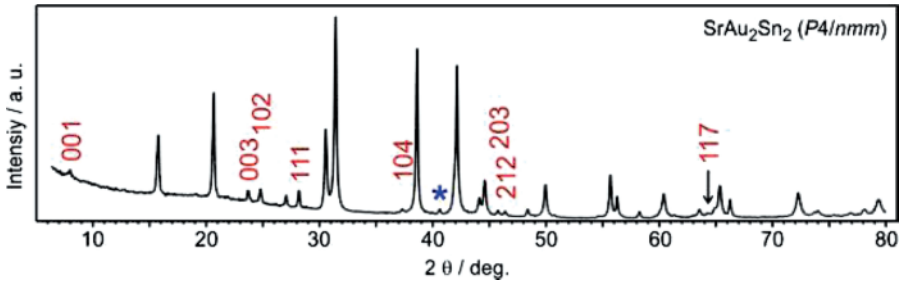

Fig. 3 (color online). Experimental powder pattern of a $SrAu_2Sn_2$ sample. The eight strongest superstructure reflections are marked with red *hkl* indices. A tiny impurity contribution is marked by a blue asterisk.

Table 3. Atomic coordinates, anisotropic and equivalent isotropic displacement parameters (pm^2) for $SrAu_xSn_{4-x}$, spacegroup $P4/nmm$. Coefficients U_{ij} of the anisotropic displacement factor tensor of the atoms are defined by: $-2\pi^2[(ha^*)^2U_{11}+\ldots+2hka^*b^*U_{12}]$; $U_{11}=U_{22}$; $U_{12}=U_{13}=U_{23}=0$; U_{eq} is defined as one third of the trace of the orthogonalized U_{ij} tensor.

Atom	Site	Occ.	x	y	z	U_{11}	U_{33}	U_{eq}
$SrAu_{1.76}Sn_{2.24}$								
Sr	2*c*	1	1/4	1/4	0.74568(16)	246(5)	216(7)	236(3)
Au1	2*b*	0.76(1)	3/4	1/4	1/2	409(5)	228(5)	348(3)
Sn1	2*b*	0.24(1)						
Au2	2*c*	1	1/4	1/4	0.13820(7)	262(3)	189(3)	237(2)
Sn3	2*a*	1	3/4	1/4	0	199(4)	180(5)	192(2)
Sn4	2*c*	1	1/4	1/4	0.37074(16)	519(7)	222(7)	420(4)
$SrAu_2Sn_2$								
Sr	2*c*	1	1/4	1/4	0.7412(3)	339(6)	336(10)	338(4)
Au1	2*b*	1	3/4	1/4	1/2	450(6)	360(6)	420(3)
Au2	2*c*	1	1/4	1/4	0.13741(10)	384(5)	351(5)	373(3)
Sn3	2*a*	1	3/4	1/4	0	316(8)	324(9)	318(5)
Sn4	2*c*	1	1/4	1/4	0.37322(17)	402(9)	368(10)	390(5)
$SrAu_{2.16}Sn_{1.84}$ (crystal A)								
Sr	2*c*	1	1/4	1/4	0.74543(13)	141(3)	179(6)	154(3)
Au1	2*b*	0.96(1)	1/4	1/4	0.13785(7)	232(3)	270(4)	245(2)
Sn1	2*b*	0.04(1)						
Au2	2*c*	1	3/4	1/4	1/2	274(3)	226(4)	258(2)
Sn3	2*a*	0.80(1)	3/4	1/4	0	249(5)	182(6)	226(3)
Au3	2*a*	0.20(1)						
Sn4	2*c*	1	1/4	1/4	0.37270(12)	208(4)	262(6)	226(3)
$SrAu_{2.16}Sn_{1.84}$ (crystal B)								
Sr	2*c*	1	1/4	1/4	0.74654(14)	193(4)	198(6)	195(3)
Au1	2*b*	0.96(2)	3/4	1/4	1/2	324(3)	242(4)	297(2)
Sn1	2*b*	0.04(2)						
Au2	2*c*	0.96(2)	1/4	1/4	0.13768(7)	303(4)	305(4)	304(2)
Sn2	2*c*	0.04(2)						
Sn3	2*a*	0.76(1)	3/4	1/4	0	326(5)	201(5)	284(3)
Au3	2*a*	0.24(1)						
Sn4	2*c*	1	1/4	1/4	0.37198(12)	269(5)	303(7)	280(3)
$SrAu_{2.22}Sn_{1.78}$								
Sr	2*c*	1	1/4	1/4	0.74636(14)	245(5)	262(7)	251(3)
Au1	2*b*	1	3/4	1/4	1/2	389(4)	297(4)	359(2)
Au2	2*c*	0.97(1)	1/4	1/4	0.13762(8)	366(4)	357(5)	363(3)
Sn2	2*c*	0.03(1)						
Sn3	2*a*	0.75(1)	3/4	1/4	0	382(6)	260(6)	342(4)
Au3	2*a*	0.25(1)						
Sn4	2*c*	1	1/4	1/4	0.37215(13)	311(5)	355(7)	326(3)

Table 4. Interatomic distances (pm) for $SrAu_2Sn_2$. Standard deviations are equal to or smaller than 0.4 pm. All distances of the first coordination spheres are listed.

Sr:	4	Sn4	355.3	Au2:	1	Sn4	267.2
	4	Au2	358.3		4	Sn3	281.0
	4	Au1	359.8		4	Sr	358.3
	4	Sn3	375.2	Sn3:	4	Au2	281.0
Au1:	4	Sn4	274.5		4	Sn3	330.8
	4	Au1	330.8		4	Sr	375.2
	4	Sr	359.8	Sn4:	1	Au2	267.2
					4	Au1	274.5
					4	Sr	355.3

The starting atomic parameters were first deduced by the charge-flipping algorithm of SUPERFLIP [18]. It was readily evident that all five crystals showed the $CaBe_2Ge_2$-type structure [19], and for the final cycles the setting of isotypic $CeIr_2P_2$ [20] was used. The refinement of the structures with anisotropic displacement parameters for all atoms on F^2 was performed with JANA2006 [21]. In order to obtain the correct compositions, the occupancy parameters of all atoms were refined in a separate series of least-squares cycles. The observed deviations from the ideal occupancies were assumed to be due to Au-Sn mixing on the respective sites. Their occupancy parameters were therefore refined as least-squares variables (Au-Sn mixing) leading to the compositions listed in Table 2. All remaining sites were fully occupied within three standard deviations and fixed in the final refinement cycles. The final difference Fourier syntheses revealed no significant residual peaks. The slightly enhanced residual electron densities are certainly a consequence of the high absorption coefficients. The final atomic positions, anisotropic and equivalent isotropic displacement parameters of all compounds as well as the interatomic distances of $SrAu_2Sn_2$ are listed in Tables 3 and 4.

Further details of the crystal structure investigation may be obtained from Fachinformationszentrum Karlsruhe, 76344 Eggenstein-Leopoldshafen, Germany (fax: +49-7247-808-666; e-mail: crysdata@fiz-karlsruhe.de, http://www.fiz-karlsruhe.de/request_for_deposited_data.html) on quoting the deposition number CSD-427707 ($SrAu_{1.76}Sn_{2.24}$), CSD-427711 ($SrAu_2Sn_2$), CSD-427709 ($SrAu_{2.16}Sn_{1.84}$ crystal A), CSD-427710 ($SrAu_{2.16}Sn_{1.84}$ crystal B), and CSD-427708 ($SrAu_{2.22}Sn_{1.78}$).

Magnetic susceptibility measurements

The magnetic susceptibility measurement of the $SrAu_2Sn_2$ sample was carried out on a Quantum Design Physical Property Measurement System using the VSM option. 25.748 mg of the polycrystalline sample was packed in a polypropylene capsule and attached to a sample holder rod for the magnetic measurement. The measurement was performed in the temperature range of 3 – 305 K with magnetic flux densities of 10 Oe and 10 kOe ($1\ \mathrm{kOe} = 7.96 \times 10^4\ \mathrm{A\,m^{-1}}$).

^{119}Sn Mössbauer spectroscopy

A $Ca^{119m}SnO_3$ source was used for the Mössbauer spectroscopic experiment. The measurement was carried out at ambient temperature in transmission geometry. The Mössbauer source was kept at room temperature. 100 mg of $SrAu_2Sn_2$ was enclosed in a small PMMA container. A palladium foil of 0.05 mm thickness was used to reduce Sn*K* X-rays concurrently emitted by this source. Fitting of the spectrum was performed with the NORMOS-90 program system [22].

Discussion

Crystal chemistry

The investigation of samples of the solid solutions $SrAu_xSn_{4-x}$ ($1.7 \leq x \leq 2.2$) by powder and single-crystal X-ray diffraction revealed isotypism with $CaBe_2Ge_2$ [19], space group $P4/nmm$. Earlier studies for $SrAu_xSn_{4-x}$ ($1.3 \leq x \leq 2.2$) reported the $BaAl_4$ type [17], space group $I4/mmm$, with gold-tin mixing on both sites of the polyanionic network. Either the weak superstructure reflections have been overlooked in that study, or the differences result from a different thermal treatment of the samples. In any case, it is remarkable that the electronic structure calculations by Tkachuk and Mar clearly pointed to higher stability of the $CaBe_2Ge_2$ type for ordered $SrAu_2Sn_2$ as observed experimentally herein. We draw back to this discrepancy later when discussing the ^{119}Sn Mössbauer spectrum.

Of the five structures refined herein we discuss only the ordered one of $SrAu_2Sn_2$. The unit cell is presented in Fig. 4. The gold and tin atoms build up a three-dimensional $[Au_2Sn_2]^{2-}$ polyanionic network in which the strontium atoms fill cages of coordination number 16 (8 Au + 8 Sn atoms). The Au–Sn distances within the network range from 267 to 281 pm, close to the sum of the covalent radii for gold and tin of 274 pm [23]. This is indicative of substantial Au–Sn bonding within the $[Au_2Sn_2]^{2-}$ polyanionic network. Similar ranges of Au–Sn distances occur in the stannides EuAuSn (276 – 283 pm) [24], $Eu_2Au_2Sn_5$ (272 – 285 pm) [25], or CeAuSn (280 pm) [26].

The $[Au_2Sn_2]^{2-}$ polyanionic network contains four crystallographically independent atoms, Au1,

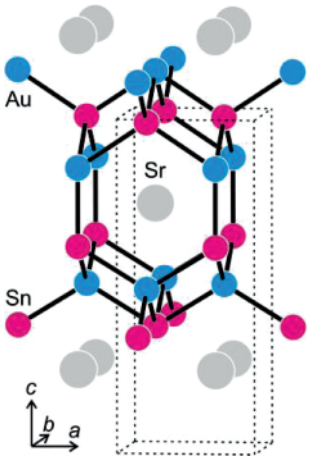

Fig. 4 (color online). The crystal structure of $SrAu_2Sn_2$ ($CaBe_2Ge_2$ type, space group $P4/nmm$) viewed approximately along the b axis. The polyanionic $[Au_2Sn_2]^{2-}$ network is emphasized.

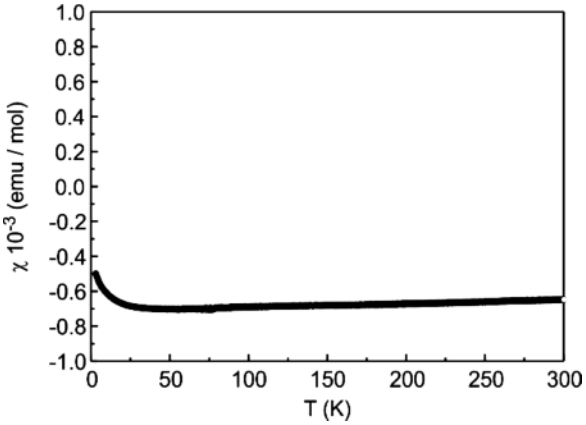

Fig. 5. Temperature-dependent magnetic susceptibility of $SrAu_2Sn_2$ measured with a magnetic field of 10 kOe.

Au2, Sn3, and Sn4. For each of these atoms heteroatomic bonding dominates. The shortest Au1–Au1 and Sn3–Sn3 contacts at 331 pm correspond to half the diagonal of the square ground plane. The Au1–Au1 distances are significantly longer than in *fcc* gold (288 pm) [27], and we can expect only weak Au1–Au1 interactions, similar as in many other $BaAl_4$-related materials [28]. The same holds true for Sn3, keeping the Sn–Sn distances of 302 (4×) and 318 pm (2×) of β-Sn [27] in mind. In the ordered variant $ThCr_2Si_2$, one would observe formation of Sn_2 pairs. Only few examples, like $BaAg_2Sn_2$ (282 pm Sn–Sn) [29] or $BaMn_2Sn_2$ (294 pm Sn–Sn), with remarkably short Sn–Sn distances are known [30]. In most cases, with the large p elements the $CaBe_2Ge_2$ type is formed, avoiding direct contact between these elements. This is especially the case when proceeding from phosphides, *via* arsenides and antimonides, to bismuthides.

The coordination of the two crystallographically independent tin atoms is important for the understanding of the ^{119}Sn Mössbauer spectrum (*vide infra*). The Sn3 atoms (Wyckoff site 2*a*, site symmetry ($\bar{4}m2$) have tetrahedral gold coordination while the Sn4 atoms have five gold neighbors in square-pyramidal coordination (2*c*, 4*mm*).

The large family of $ThCr_2Si_2$- and $CaBe_2Ge_2$-type intermetallics has repeatedly been reviewed [25, 28, 31 – 33]. For further details we refer to these overviews.

Magnetic properties of $SrAu_2Sn_2$

Fig. 5 depicts the temperature dependence of the magnetic susceptibility of $SrAu_2Sn_2$ in the temperature range 3 – 300 K (10 kOe data). Above 25 K it can be considered fairly independent of temperature with the Curie tail being attributed to a minor paramagnetic impurity. $SrAu_2Sn_2$ can be considered as a diamagnetic material with a temperature independent susceptibility of $\chi_{Dia} = -0.65(5) \times 10^{-3}$ emu mol^{-1}. An additional measurement at 10 Oe gave no hint for a superconducting transition.

^{119}Sn Mössbauer spectroscopy of $SrAu_2Sn_2$

The ^{119}Sn Mössbauer spectrum of the $SrAu_2Sn_2$ sample at room temperature is presented in Fig. 6 together with a transmission integral fit. In agreement with the two crystallographically independent tin sites observed in the structure refinement, the spectrum could be well reproduced with a superposition of two signals. The first signal occurs at an isomer shift of $\delta = 2.23(3)$ mm s^{-1}, subjected to quadrupole splitting of $\Delta E_Q = 0.72(5)$ mm s^{-1} and an experimental line width of $\Gamma = 0.72(3)$ mm s^{-1}. The second signal has the fit parameters $\delta = 1.93(6)$ mm s^{-1}, $\Delta E_Q = 0.2(2)$ mm s^{-1} and $\Gamma = 0.91(7)$ mm s^{-1}. These two spectral components occur in a ratio of 60 : 40, although one would expect a 50 : 50 ratio based on the two Wyckoff sites 2*a* and 2*c*. Assignment of the two signals to the Sn3 and Sn4 atoms is feasible through the coordination with gold discussed above. The first

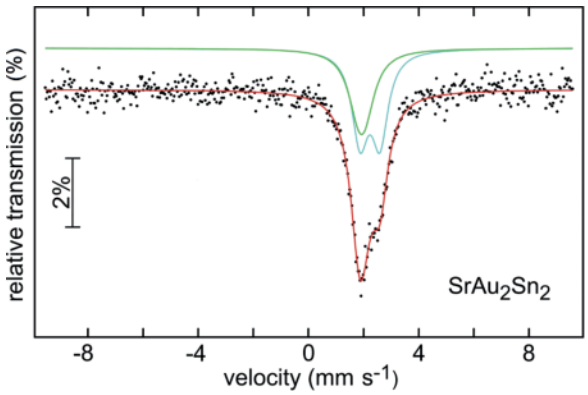

Fig. 6 (color online). Experimental (data points) and simulated (continuous lines) ^{119}Sn Mössbauer spectrum of $SrAu_2Sn_2$ at room temperature. For details see text.

signal with the larger quadrupole splitting results from the Sn4 atoms with the square-pyramidal gold coordination which shows higher asymmetry as compared to the distorted tetrahedral Sn3Au$_4$ coordination. The Sn4 atoms show a slightly higher isomer shift, indicating slightly higher *s* electron density at these tin nuclei as compared to Sn3. These isomer shifts are in the typical range for tin intermetallics [7, 15, 25, 26, 34].

Finally we draw back to the intensities of the two sub-spectra. We observe higher intensity for the signal of the atoms with square-pyramidal coordination. This is indicative of substantial disorder in the bulk $SrAu_2Sn_2$ sample and means that several domains show tin preferentially on these square-pyramidal sites. This can readily be rationalized also from the refined occupancy parameters of the other four data sets. Such disorder has also been observed for bulk samples of CeT_2Sn$_2$ (T = Cu, Pd, Pt) [35, 36] and $SmCu_2Sn_2$ [35].

The Au-Sn disorder is certainly a function of the x value for the $SrAu_xSn_{4-x}$ samples, but also strongly depends on the thermal treatment. This might explain the absence of superstructure reflections observed in the earlier study, pointing to even higher degrees of disorder.

Conclusion

Powder and single-crystal X-ray diffraction data clearly reveal that samples of the solid solutions $SrAu_xSn_{4-x}$ ($1.7 \leq x \leq 2.2$) crystallize with the $CaBe_2Ge_2$-type structure, space group $P4/nmm$. $SrAu_2Sn_2$ is diamagnetic. ^{119}Sn Mössbauer spectroscopic data of a $SrAu_2Sn_2$ sample indicate substantial disorder (Au-Sn mixing). This is also evident from single-crystal data with x values smaller or larger than 2.

Acknowledgement

We thank Dipl.-Ing. Ute Ch. Rodewald for the intensity data collections. This work was supported by the Deutsche Forschungsgemeinschaft through SPP 1458 *Hochtemperatursupraleitung in Eisenpnictiden*.

[1] R. Pöttgen, *Z. Naturforsch.* **2006**, *61b*, 677.
[2] C. J. Evans, *Tin Handbook*, 3rd ed., Hüthig, Heidelberg, **1994**.
[3] U. Eberz, W. Seelentag, H.-U. Schuster, *Z. Naturforsch.* **1980**, *35*, 1341.
[4] D. Kußmann, R.-D. Hoffmann, R. Pöttgen, *Z. Anorg. Allg. Chem.* **1998**, *624*, 1727.
[5] Q. Lin, J. D. Corbett, *Inorg. Chem.* **2011**, *50*, 1808.
[6] Q. Lin, J. D. Corbett, *Inorg. Chem.* **2010**, *49*, 10436.
[7] R.-D. Hoffmann, R. Pöttgen, D. Kußmann, D. Niepmann, H. Trill, B. D. Mosel, *Solid State Sci.* **2002**, *4*, 481.
[8] S. Esmailzadeh, R.-D. Hoffmann, R. Pöttgen, *Z. Naturforsch.* **2004**, *59b*, 1451.
[9] A. V. Tkachuk, A. Mar, *J. Solid State Chem.* **2007**, *180*, 2298.
[10] I. Schellenberg, R.-D. Hoffmann, S. Seidel, C. Schwickert, R. Pöttgen, *Z. Naturforsch.* **2011**, *66b*, 985.
[11] I. Schellenberg, R.-D. Hoffmann, C. Schwickert, R. Pöttgen, *Solid State Sci.* **2011**, *13*, 1740.
[12] S. Seidel, R.-D. Hoffmann, R. Pöttgen, *Z. Kristallogr.* **2014**, *229*, in press.
[13] C. Schwickert, R.-D. Hoffmann, F. Winter, R. Pöttgen, *Z. Kristallogr.* **2014**, *229*, in press.
[14] R. Pöttgen, Th. Gulden, A. Simon, *GIT Labor-Fachzeitschrift* **1999**, *43*, 133.
[15] R. Pöttgen, A. Lang, R.-D. Hoffmann, B. Künnen, G. Kotzyba, R. Müllmann, B. D. Mosel, C. Rosenhahn, *Z. Kristallogr.* **1999**, *214*, 143.
[16] K. Yvon, W. Jeitschko, E. Parthé, *J. Appl. Crystallogr.* **1977**, *10*, 73.
[17] K. R. Andress, E. Alberti, *Z. Metallkd.* **1935**, *27*, 126.

[18] L. Palatinus, G. Chapuis, *J. Appl. Crystallogr.* **2007**, *40*, 786.
[19] B. Eisenmann, N. May, W. Müller, H. Schäfer, *Z. Naturforsch.* **1972**, *27b*, 1155.
[20] U. Pfannenschmidt, F. Behrends, H. Lincke, M. Eul, K. Schäfer, H. Eckert, R. Pöttgen, *Dalton Trans.* **2012**, *41*, 14188.
[21] V. Petříček, M. Dušek, L. Palatinus, *Z. Kristallogr.* **2014**, *229*, 345.
[22] R. A. Brand, NORMOS, Mössbauer fitting Program, Universität Duisburg, Duisburg (Germany) **2007**.
[23] J. Emsley, *The Elements*, Oxford University Press, Oxford **1999**.
[24] R. Pöttgen, R.-D. Hoffmann, R. Müllmann, B. D. Mosel, G. Kotzyba, *Chem. Eur. J.* **1997**, *3*, 1852.
[25] D. Kußmann, R. Pöttgen, U. Ch. Rodewald, C. Rosenhahn, B. D. Mosel, G. Kotzyba, B. Künnen, *Z. Naturforsch.* **1999**, *54b*, 1155.
[26] D. Niepmann, R. Pöttgen, K. M. Poduska, F. J. DiSalvo, H. Trill, B. D. Mosel, *Z. Naturforsch.* **2001**, *56b*, 1.
[27] J. Donohue, The Structures of the Elements, Wiley, New York, **1974**.
[28] D. Johrendt, C. Felser, O. Jepsen, O. K. Andersen, A. Mewis, J. Rouxel, *J. Solid State Chem.* **1997**, *130*, 254.
[29] N. May, H. Schäfer, *Z. Naturforsch.* **1972**, *27b*, 864.
[30] W. Dörrscheidt, N. Niess, H. Schäfer, *Z. Naturforsch.* **1976**, *31b*, 890.
[31] C. Zheng, R. Hoffmann, *J. Solid State Chem.* **1988**, *72*, 58.
[32] E. Parthé, L. Gelato, B. Chabot, M. Penzo, K. Cenzual, R. Gladyshevskii, *TYPIX-Standardized Data and Crystal Chemical Characterization of Inorganic Structure Types*, Gmelin Handbook of Inorganic and Organometallic Chemistry, 8th edition, Springer, Berlin, **1993**.
[33] R. Pöttgen, *Z. Anorg. Allg. Chem.* **2014**, *640*, 869.
[34] R. Mishra, R. Pöttgen, R.-D. Hoffmann, H. Trill, B. D. Mosel, H. Piotrowski, M. F. Zumdick, *Z. Naturforsch.* **2001**, *56b*, 589.
[35] E. A. Görlich, K. Latka, J. Moser, *Hyp. Int.* **1989**, *50*, 723.
[36] E. Lidström, A. M. Ghandour, L. Häggström, Y. Andersson, *J. Alloys Compd.* **1996**, *232*, 95.